1 # Small molecule inhibition of METTL3 as a strategy against myeloid
2 leukaemia
3
4 Eliza Yankova[1,2,3*], Wesley Blackaby[3*], Mark Albertella[3], Justyna Rak[2,4], Etienne De
5 Braekeleer[2,4], Georgia Tsagkogeorga[1,3], Ewa S. Pilka[5], Demetrios Aspris[2,6], Dan Leggate[3],
6 Alan G. Hendrick[3], Natalie A. Webster[3], Byron Andrews[3], Richard Fosbeary[3], Patrick Guest[3],
7 Nerea Irigoyen[7], Maria Eleftheriou[1], Malgorzata Gozdecka[2], Joao M. L. Dias[8], Andrew J.
8 Bannister[12], Binje Vick[9,10], Irmela Jeremias[9,10,11], George S. Vassiliou[2,4,6], Oliver Rausch[3+],
9 Konstantinos Tzelepis[1,2,4,12+], Tony Kouzarides[1,12+]
10
11 1. Milner Therapeutics Institute, University of Cambridge, Puddicombe Way,
12 Cambridge, CB2 0AW, UK
13 2. Haematological Cancer Genetics, Wellcome Trust Sanger Institute, Hinxton,
14 Cambridge, CB10 1SA, UK
15 3. Storm Therapeutics Ltd, Babraham Research Campus, Cambridge, CB22 3AT, UK
16 4. Wellcome-MRC Cambridge Stem Cell Institute, University of Cambridge,
17 Puddicombe Way, Cambridge, CB2 0AW, UK
18 5. Evotec (UK) Ltd, Milton Park, Abingdon, OX14 4RZ, UK
19 6. The Center for the Study of Hematological Malignancies/Karaiskakio
20 Foundation, Nicandrou Papamina Avenue, 2032 Nicosia, Cyprus
21 7. Division of Virology, Department of Pathology, University of Cambridge,
22 Cambridge, CB2 1QP, UK
23 8. MRC Cancer Unit, University of Cambridge, Hutchison/MRC Research Centre,
24 Cambridge Biomedical Campus, Cambridge, CB2 0XZ, UK
25 9. Research Unit Apoptosis in Hematopoietic Stem Cells, Helmholtz Zentrum München,
26 German Research Center for Environmental Health (HMGU), 81377, Munich,
27 Germany
28 10. German Consortium for Translational Cancer Research (DKTK), Partnering Site
29 Munich, 81377, Munich, Germany
30 11. Department of Pediatrics, Dr. von Hauner Children's Hospital, Ludwig Maximilians
31 University München, 80337, Munich, Germany
32 12. The Gurdon Institute and Department of Pathology, University of Cambridge, Tennis
33 Court Road, Cambridge, CB2 1QN, UK
34
35 *These authors contributed equally to this work
36
37 + Correspondence:
38 -Tony Kouzarides (t.kouzarides@gurdon.cam.ac.uk)
39 -Konstantinos Tzelepis (kt404@cam.ac.uk)
40 -Oliver Rausch (oliver.rausch@stormtherapeutics.com)
41
42
43 The N6-methyladenosine (m^6A) is an abundant internal RNA modification[1,2] catalysed
44 predominantly by the METTL3–METTL14 methyltransferase complex[3,4]. The m^6A writer
45 METTL3 has been linked to the initiation and maintenance of acute myeloid leukaemia (AML),
46 but its true therapeutic importance is still unknown[5-7]. Here we present the identification and
47 characterisation of a highly potent and selective first-in-class catalytic inhibitor of METTL3
48 (STM2457) and its co-crystal structure bound to METTL3/METTL14. Treatment with

49 STM2457 leads to reduced AML growth, and an increase in differentiation and apoptosis.
50 These cellular effects are accompanied by selective reduction of m^6A levels on known
51 leukaemogenic mRNAs and a decrease in their expression consistent with a translational
52 defect. We demonstrate that pharmacological inhibition of METTL3 *in vivo* leads to impaired
53 engraftment and prolonged survival in various AML mouse models, specifically targeting key
54 stem cell subpopulations of AML. Collectively, these results reveal the inhibition of METTL3
55 as a potential therapeutic strategy against AML, and provide proof of concept that the targeting
56 of RNA modifying enzymes represents a promising new avenue for anti-cancer therapy.

57

58 **Main**

59 To investigate the therapeutic potential of targeting the enzymatic activity of METTL3 as an
60 anti-leukaemic strategy, we developed the small molecule STM2457. A high throughput screen
61 (HTS) of 250,000 diverse drug-like compounds was carried out. STM1760 [half maximum
62 inhibitory concentration (IC_{50}) = 51.7 μM] was one of only two non-S-adenosyl methionine
63 (SAM) related hits arising from the HTS (Extended Data Fig. 1a, b). After optimisation of
64 potency, *in vitro* ADME and *in vivo* pharmacokinetic properties, we identified STM2457 (Fig.
65 1a). STM2120 (IC_{50} = 64.5 μM) was identified as structurally related, but 1,000 fold less active
66 compared to STM2457 (Fig. 1b and Extended Data Fig. 1a).

67

68 **Characterisation of STM2457**

69 STM2457 is a potent inhibitor of METTL3/METTL14 catalytic activity with a IC_{50} of 16.9 nM
70 (Fig. 1b). Direct binding to the METTL3/METTL14 heterodimer was confirmed using surface
71 plasmon resonance (SPR) with a high affinity Kd of 1.4 nM (Fig. 1c, d and Extended Data Fig.
72 1c-e). A co-factor competitive binding mode was demonstrated using SAM in the SPR running
73 buffer (Fig. 1d). There was no evidence that the compound disrupted the METTL3/METTL14
74 complex. STM2457 is highly specific for METTL3 and showed no inhibition of other RNA
75 methyltransferases (Extended Data Fig. 1f). Moreover, STM2457 showed >1,000-fold
76 selectivity for METTL3 when tested against a broad panel of 45 RNA, DNA and protein
77 methyltransferases (Fig. 1e and Extended Data Fig. 1g), and showed no inhibitory effect on a
78 panel of 468 kinases (Extended Data Fig. 1h). We further characterized the binding of
79 STM2457 to METTL3 by X-ray crystallography, confirming the binding of STM2457 to the
80 SAM binding site (Fig. 1f and Extended Data Fig. 2a). The strong selectivity of STM2457
81 observed in the methyltransferase panel is consistent with: the structural dissimilarity with
82 SAM or known methyl transferase inhibitors, its avoidance of the homocysteine binding pocket
83 utilized by SAM, the reorganization of K513 on STM2457 binding, and the known structural
84 diversity of the cofactor binding site of SAM-dependent methyl transferases[8].
85 Equipotent inhibition of human and mouse METTL3 by STM2457 was demonstrated using a
86 cellular thermal-shift assay (Extended Data Fig. 2b). The difference between biochemical and
87 cellular IC_{50} of STM2457 is consistent with the Km of SAM for METTL3/14 (0.1 μM)[9] and
88 the competition from highly abundant intracellular SAM[10]. We further demonstrated target
89 inhibition of STM2457 in cells by measuring concentration-dependent reduction of m^6A on
90 poly-A^+-enriched RNA (Fig. 1g and Extended Data Fig. 2c). No changes were detected on
91 other RNA modifications (Extended Data Fig. 2d). Pharmacokinetic profiling of STM2457 in
92 mice following a single intra-peritoneal dose of 50 mg/kg indicated a sufficient half-life of
93 STM2457, ensuring appropriate compound exposure levels *in vivo* over 24h (Extended Data
94 Fig. 2e). Dose-dependent inhibition of m^6A on poly-A^+-enriched RNA from mouse spleens
95 confirmed a clear relationship between compound exposure and target inhibition *in vivo*

(Extended Data Fig. 2f). These data demonstrate that STM2457 is a highly potent, specific and bioavailable inhibitor of METTL3, suitable for *in vivo* investigations.

Cellular and molecular effects of STM2457

To study the anti-leukaemic potential of STM2457 we examined the proliferation of a panel of human AML cell lines post-treatment and detected significant growth reduction in a concentration-dependent manner (Fig. 2a) while we found that STM2457 did not affect the colony-forming ability of normal human cord blood CD34$^+$ cells (Extended Data Fig. 3a). We also observed no impact on the proliferation of MOLM-13 cells treated with the control small molecule STM2120, unlike our observations with STM2457 (Extended Data Fig. 3b). Additionally, treatment with STM2457 significantly reduced the clonogenic potential of primary murine AML cells (Fig. 2b and Extended Data Fig. 3c), while having no effect on normal haematopoietic stem and progenitor cells (HSPCs) (Fig. 2c). Pharmacological inhibition of METTL3 also caused significant myeloid differentiation[6,11] and cell cycle arrest in MOLM-13 and primary murine AML cells (Fig. 2d, e). In contrast, the same effects were not identified using the non-leukaemic haemopoietic cell line HPC7 (Fig. 3e and Extended Data Fig. 3d). Moreover, treatment with STM2457 induced apoptosis in human and mouse AML models but not in normal non-leukaemic haemopoietic cells (Fig. 2f and Extended Data Fig. 3e). To assess the impact of pharmacological inhibition of METTL3 on two known METTL3 biomarkers associated with AML, SP1[6,12] and BRD4[13,14], we treated MOLM-13 cells with STM2457 and observed a dose-dependent reduction of SP1 and BRD4 protein levels (Fig. 2g). Notably, ectopic expression of SP1 significantly reduced the sensitivity of MOLM-13 cells to STM2457 (Extended Data Fig. 3f, g). These data establish that the catalytic function of METTL3 is important for leukaemia growth, in line with previous findings[6,7,15].

We next sought to investigate the molecular mechanism by which STM2457 affects AML. RNAseq analysis of MOLM-13 cells treated with STM2457 revealed 1,338 up-regulated and 489 down-regulated genes (Extended Data Fig. 4a and Supplementary Table 1). Gene ontology (GO) analysis of the differentially expressed genes showed enrichment in pathways related to myeloid differentiation, cell cycle and leukaemia progression (Extended Data Fig. 4b, c) in close agreement with our phenotypic observations (Supplementary Table 2). To examine the impact of the pharmacological inhibition of METTL3 on m^{6}A levels we performed m^{6}A-meRIP-seq in MOLM-13 cells treated with STM2457. This identified 11,909 m^{6}A peaks on poly-A$^+$-enriched RNA, of which 4,666 were reduced upon STM2457 treatment, indicating that they were METTL3-catalytic dependent (Fig. 3a and Supplementary Table 3). We observed no major changes between the general m^{6}A distribution and the distribution upon treatment with STM2457 (Fig. 3a, b). Importantly, motif analysis identified the m^{6}A-associated DRACH motif[16] as the top candidate (Fig. 3c), validating the specificity of STM2457.

We next compared our m^{6}A-meRIP-seq findings to previously published meRIP-seq dataset[6] using METTL3 knock-down (KD) in MOLM-13 cells. This analysis identified a significant overlap in the differentially m^{6}A-methylated poly-A$^+$ RNAs as well as in the differential m^{6}A peaks (Extended Data Fig. 5a, b and Supplementary Table 4), including many known and novel METTL3-specific m^{6}A substrates (Fig. 3d and Extended Data Fig. 5c). The substrate and peak differences observed could be attributed to the more specific catalytic inhibition of METTL3 by STM2457 compared to prolonged METTL3 KD which potentially disrupts the overall m^{6}A methyltransferase complex[17]. m^{6}A-meRIP and qPCR validation revealed that treatment with STM2457 leads to reduced m^{6}A levels in METTL3-dependent core leukaemogenic m^{6}A substrates including *HOXA10*[18] and *MYC*[19], while no difference observed in METTL3-independent m^{6}A substrates (Extended Data Fig. 5d), thus validating the specificity of our m^{6}A

145 profiling. GO analysis of the differential m^6A-meRIP candidates revealed enrichment of
146 pathways involved in chromatin modification, DNA damage and RNA splicing (Extended Data
147 Fig. 5e and Supplementary Table 5). These findings are consistent with a nuclear function for
148 METTL3 catalytic activity, bolstering the previously reported chromatin-based mechanism
149 required for AML cell survival[6], and the connections of m^6A with nuclear biological
150 processes[20-22].
151
152 We and others have shown that genetic inhibition of *METTL3* and *METTL14* leads to mRNA
153 translational defects and ribosomal stalling[6,7,15,23]. We therefore examined whether isolated
154 catalytic inhibition of METTL3 causes similar translational defects. Polysome profiling
155 revealed loss of high polysome fractions following treatment with STM2457 in MOLM-13
156 cells (Fig. 3e). Validation of the polysome fractions using qPCR indicated a significant
157 reduction of known METTL3-dependent substrates in the high molecular weight fractions and
158 an increase in the lower, suggesting ribosomal stalling (Fig. 3f). In contrast, a METTL3-
159 independent m^6A substrate, *DICER1*, remained unaffected by the treatment with STM2457
160 (Fig. 3f). Crucially, the overall RNA expression levels of the METTL3 biomarkers *BRD4* and
161 *SP1* showed no alterations (Fig. 3g), while protein levels were greatly reduced (Fig. 2g),
162 verifying that the effects on mRNA are at the translational and not at the transcriptional level.
163 Furthermore, treatment with STM2457 maintained the expression levels of *METTL3* or
164 *DICER1* (Extended Data Fig. 5f) as well as the protein levels of METTL3, METTL14, DDX3X
165 and DICER1 (Extended Data Fig. 5g) further suggesting that the impact on mRNA translation
166 is not global but rather specific. Altogether, this mechanistic analysis illustrates that catalytic
167 inhibition of METTL3 causes gene expression defects consistent with an effect on the mRNA
168 translational efficiency of m^6A substrates.
169
170 **In vivo efficacy of STM2457**
171 Following the positive evidence for strong pharmacological inhibition of METTL3 *in vitro,* we
172 performed *in vivo* studies using clinically relevant AML models. Initially, we utilised 3 human
173 AML patient derived xenografts (PDX) of different genotypes. Daily treatment with STM2457
174 led to impairment of engraftment and AML expansion *in vivo* and significantly prolonged the
175 mouse lifespan (Fig. 4a-d and Extended Data Fig. 6a-e) with no overt toxicity or effect on
176 mouse body weight (Extended Data Fig. 6f). The anti-leukaemic effect was also confirmed by
177 the reduction of human $CD45^+$ cells in bone marrow and spleen following treatment (Fig. 4e).
178 Effective METTL3 target inhibition by STM2457 *in vivo* was demonstrated by the selective
179 reduction of key METTL3 m^6A substrates at the protein level while METTL3 levels remained
180 unchanged (Extended Data Fig. 6g). Additionally, total m^6A levels on poly-A^+-enriched RNA
181 were significantly reduced following treatment with STM2457 (Extended Data Fig. 6h). In
182 parallel with the PDX models, we used a primary murine *MLL-AF9/$Flt3^{Itd/+}$ in vivo* model with
183 similar anti-leukaemic observations regarding reduction in the engrafted AML cells, reduction
184 in spleen size, selective reduction of METTL3 biomarkers as well as reduction of m^6A on poly-
185 A^+-enriched RNA (Extended Data Fig. 7a-d).
186
187 Having established the significant anti-leukaemic effect of STM2457 *in vivo*, we went on to
188 investigate the effect of pharmacological inhibition of METTL3 at the core leukaemia stem
189 cell level. Previous studies have shown that $CD93^+$[24] and L-GMP[25] subpopulations are directly
190 connected to generation and maintenance of primary murine and human patient AMLs driven
191 by MLL rearrangement. Interestingly, we observed that the $CD93^+$ and L-GMP populations
192 were significantly reduced following treatment with STM2457, revealing a strong dependency
193 on the catalytic function of METTL3 (Fig. 4f and Extended Data Fig. 7e, f). Furthermore,
194 $CD48^+$ intensity was increased upon treatment with STM2457 (Extended Data Fig. 7g), thus

195 revealing loss of self-renewal at the leukaemia stem cell level, in concordance with our *in vitro*
196 and *ex vivo* observations. To show that METTL3 inhibition results in functional impairment of
197 leukemic stem cells, we performed re-transplantation experiments using murine or patient-
198 derived AML cells from primary transplants treated with vehicle or STM2457. We observed a
199 significant lifespan prolongation and a marked decrease in the presence of AML cells in
200 peripheral blood, exclusively upon initial treatment with STM2457 (Fig. 4g, h and Extended
201 Data Fig. 7h, i). In summary, the pharmacological inhibition of METTL3 *in vivo* impairs AML
202 expansion by affecting the AML stem cell/leukaemia-propagating compartment.
203
204 Finally, we evaluated the potential toxicity of the established anti-leukaemic dose of STM2457
205 *in vivo*. No significant changes were observed in the numbers of bone marrow-derived
206 hematopoietic stem cells (HSCs) and early progenitors (Lin−, Sca1+, Kit+), peripheral blood
207 counts or mouse body weight (Extended Data Fig. 8a-e). We also confirmed effective catalytic
208 inhibition of METTL3 as the m^6A levels on poly-A^+-enriched RNA were significantly reduced
209 after treatment with STM2457 (Extended Data Fig. 8f). These data suggest that small molecule
210 inhibition of METTL3 is detrimental for the maintenance of AML, but has no significant or
211 lasting impact on normal haematopoiesis.
212
213 Here we present the characterisation of STM2457, the first bioavailable inhibitor of the m^6A
214 writer METTL3. Critically, we show that catalytic inhibition of METTL3 via STM2457 targets
215 key stem cell populations of AML which reverses the AML phenotype, preventing or
216 prolonging the development of AML in re-transplantation experiments. Hence, our findings
217 present a promising targeting strategy of the leukemic stem cell subpopulation responsible for
218 AML persistence/recurrence and provide a rationale for future investigations of combined
219 pharmacological inhibition of METTL3 with mainstream anti-AML therapies[26,27]. Overall, our
220 efforts further highlight the impact of m^6A hijacking on the AML status, as previously
221 shown[6,7,28-30]. To our knowledge, this is the first study demonstrating *in vivo* activity and
222 therapeutic efficacy of inhibitors of an RNA methyltransferase against cancer.
223
224
225
226 **References**
227
228 1 Dominissini, D. *et al.* Topology of the human and mouse m6A RNA methylomes
229 revealed by m6A-seq. *Nature* **485**, 201-206, doi:10.1038/nature11112 (2012).
230 2 Meyer, K. D. *et al.* Comprehensive analysis of mRNA methylation reveals
231 enrichment in 3' UTRs and near stop codons. *Cell* **149**, 1635-1646,
232 doi:10.1016/j.cell.2012.05.003 (2012).
233 3 Liu, J. *et al.* A METTL3-METTL14 complex mediates mammalian nuclear RNA N6-
234 adenosine methylation. *Nat Chem Biol* **10**, 93-95, doi:10.1038/nchembio.1432 (2014).
235 4 Wang, X. *et al.* Structural basis of N(6)-adenosine methylation by the METTL3-
236 METTL14 complex. *Nature* **534**, 575-578, doi:10.1038/nature18298 (2016).
237 5 Tzelepis, K. *et al.* A CRISPR Dropout Screen Identifies Genetic Vulnerabilities and
238 Therapeutic Targets in Acute Myeloid Leukemia. *Cell Rep* **17**, 1193-1205,
239 doi:10.1016/j.celrep.2016.09.079 (2016).
240 6 Barbieri, I. *et al.* Promoter-bound METTL3 maintains myeloid leukaemia by m(6)A-
241 dependent translation control. *Nature* **552**, 126-131, doi:10.1038/nature24678 (2017).
242 7 Vu, L. P. *et al.* The N(6)-methyladenosine (m(6)A)-forming enzyme METTL3
243 controls myeloid differentiation of normal hematopoietic and leukemia cells. *Nat Med*
244 **23**, 1369-1376, doi:10.1038/nm.4416 (2017).

245 8 Schapira, M. Structural Chemistry of Human RNA Methyltransferases. *ACS Chem*
246 *Biol* **11**, 575-582, doi:10.1021/acschembio.5b00781 (2016).
247 9 Li, F. *et al.* A Radioactivity-Based Assay for Screening Human m6A-RNA
248 Methyltransferase, METTL3-METTL14 Complex, and Demethylase ALKBH5. *J*
249 *Biomol Screen* **21**, 290-297, doi:10.1177/1087057115623264 (2016).
250 10 Melnyk, S., Pogribna, M., Pogribny, I. P., Yi, P. & James, S. J. Measurement of
251 plasma and intracellular S-adenosylmethionine and S-adenosylhomocysteine utilizing
252 coulometric electrochemical detection: alterations with plasma homocysteine and
253 pyridoxal 5'-phosphate concentrations. *Clin Chem* **46**, 265-272 (2000).
254 11 Ripperger, T. *et al.* The heteromeric transcription factor GABP activates the
255 ITGAM/CD11b promoter and induces myeloid differentiation. *Biochim Biophys Acta*
256 **1849**, 1145-1154, doi:10.1016/j.bbagrm.2015.07.005 (2015).
257 12 O'Connor, L., Gilmour, J. & Bonifer, C. The Role of the Ubiquitously Expressed
258 Transcription Factor Sp1 in Tissue-specific Transcriptional Regulation and in
259 Disease. *Yale J Biol Med* **89**, 513-525 (2016).
260 13 Choe, J. *et al.* mRNA circularization by METTL3-eIF3h enhances translation and
261 promotes oncogenesis. *Nature* **561**, 556-560, doi:10.1038/s41586-018-0538-8 (2018).
262 14 Dawson, M. A. *et al.* Inhibition of BET recruitment to chromatin as an effective
263 treatment for MLL-fusion leukaemia. *Nature* **478**, 529-533, doi:10.1038/nature10509
264 (2011).
265 15 Weng, H. *et al.* METTL14 Inhibits Hematopoietic Stem/Progenitor Differentiation
266 and Promotes Leukemogenesis via mRNA m(6)A Modification. *Cell Stem Cell* **22**,
267 191-205 e199, doi:10.1016/j.stem.2017.11.016 (2018).
268 16 Dominissini, D., Moshitch-Moshkovitz, S., Salmon-Divon, M., Amariglio, N. &
269 Rechavi, G. Transcriptome-wide mapping of N(6)-methyladenosine by m(6)A-seq
270 based on immunocapturing and massively parallel sequencing. *Nat Protoc* **8**, 176-189,
271 doi:10.1038/nprot.2012.148 (2013).
272 17 Tzelepis, K., Rausch, O. & Kouzarides, T. RNA-modifying enzymes and their
273 function in a chromatin context. *Nat Struct Mol Biol* **26**, 858-862,
274 doi:10.1038/s41594-019-0312-0 (2019).
275 18 Alharbi, R. A., Pettengell, R., Pandha, H. S. & Morgan, R. The role of HOX genes in
276 normal hematopoiesis and acute leukemia. *Leukemia* **27**, 1000-1008,
277 doi:10.1038/leu.2012.356 (2013).
278 19 Delgado, M. D. & Leon, J. Myc roles in hematopoiesis and leukemia. *Genes Cancer*
279 **1**, 605-616, doi:10.1177/1947601910377495 (2010).
280 20 Liu, J. *et al.* N (6)-methyladenosine of chromosome-associated regulatory RNA
281 regulates chromatin state and transcription. *Science* **367**, 580-586,
282 doi:10.1126/science.aay6018 (2020).
283 21 Mikutis, S. *et al.* meCLICK-Seq, a Substrate-Hijacking and RNA Degradation
284 Strategy for the Study of RNA Methylation. *ACS Central Science*,
285 doi:10.1021/acscentsci.0c01094 (2020).
286 22 Xiang, Y. *et al.* RNA m(6)A methylation regulates the ultraviolet-induced DNA
287 damage response. *Nature* **543**, 573-576, doi:10.1038/nature21671 (2017).
288 23 Lin, S., Choe, J., Du, P., Triboulet, R. & Gregory, R. I. The m(6)A Methyltransferase
289 METTL3 Promotes Translation in Human Cancer Cells. *Mol Cell* **62**, 335-345,
290 doi:10.1016/j.molcel.2016.03.021 (2016).
291 24 Iwasaki, M., Liedtke, M., Gentles, A. J. & Cleary, M. L. CD93 Marks a Non-
292 Quiescent Human Leukemia Stem Cell Population and Is Required for Development
293 of MLL-Rearranged Acute Myeloid Leukemia. *Cell Stem Cell* **17**, 412-421,
294 doi:10.1016/j.stem.2015.08.008 (2015).

295 25 Krivtsov, A. V. *et al.* Transformation from committed progenitor to leukaemia stem
296 cell initiated by MLL-AF9. *Nature* **442**, 818-822, doi:10.1038/nature04980 (2006).
297 26 Ellison, R. R. *et al.* Arabinosyl cytosine: a useful agent in the treatment of acute
298 leukemia in adults. *Blood* **32**, 507-523 (1968).
299 27 Daver, N. *et al.* New directions for emerging therapies in acute myeloid leukemia: the
300 next chapter. *Blood Cancer J* **10**, 107, doi:10.1038/s41408-020-00376-1 (2020).
301 28 Li, Z. *et al.* FTO Plays an Oncogenic Role in Acute Myeloid Leukemia as a N(6)-
302 Methyladenosine RNA Demethylase. *Cancer Cell* **31**, 127-141,
303 doi:10.1016/j.ccell.2016.11.017 (2017).
304 29 Huang, Y. *et al.* Small-Molecule Targeting of Oncogenic FTO Demethylase in Acute
305 Myeloid Leukemia. *Cancer Cell* **35**, 677-691 e610, doi:10.1016/j.ccell.2019.03.006
306 (2019).
307 30 Moroz-Omori, E. V. *et al.* METTL3 inhibitors for epitranscriptomic modulation of
308 cellular processes. *bioRxiv*, 2020.2009.2025.311803, doi:10.1101/2020.09.25.311803
309 (2020).
310
311
312
313
314 **Methods**
315
316
317 **METTL3/14 RF/MS methyltransferase assay**
318 The enzymatic assay was established to determine IC_{50} values for the inhibition of RNA
319 methyltransferase activity. The enzyme used was full-length his-tagged METTL3 co-expressed
320 with full length FLAG-tagged METTL14 in a baculovirus expression system. The enzyme
321 complex was purified using standard affinity chromatography. Enzymatic reactions were
322 performed at room temperature in 384-well plates using a final reaction volume of 20 µL
323 containing 20 mM TrisCl pH 7.6, 1 mM DTT, 0.01% Tween-20. 5 nM final concentration of
324 METTL3/14 was pre-incubated with various compound concentrations for 10 minutes,
325 followed by addition of 0.2 µM final concentration synthetic RNA substrate (5'P-
326 uacacucgaucuggacuaaagcugcuc-3') and 0.5 µM final concentration S-adenosyl methionine
327 (SAM). The reaction was incubated for further 60 minutes at room temperature, and then
328 quenched by the addition of 40 µL 7.5% TCA with internal standard. After termination, plates
329 were sealed, centrifuged and stored at 4°C until analysis.
330 METTL3 activity was assessed using the RapidFire™ mass spectrometry (RF/MS) platform to
331 measure the S-adenosyl homocysteine (SAH) product. Stopped and stable assay plates were
332 analyzed on the Agilent RF300 integrated autosampler/solid-phase extraction (SPE) system
333 coupled to an ABSciex 4000 mass spectrometer for the quantification of the SAH and
334 normalized to the ratio of signal of two internal standards. The mass transition for the product
335 (SAH) was 384.9/135.9 Da. Transitions of the internal standard were used for normalization
336 of matrix effects.
337 Compound IC_{50} values were calculated by measuring enzyme activity over a dilution series of
338 inhibitor concentrations. Percent inhibition was normalized to control wells without RNA
339 substrate and without inhibition (DMSO only). Data were evaluated using a four-parameter
340 logistic equation in GraphPad Prism (Version 9).
341
342 **X-ray crystallography: Cloning, protein expression and purification**

343 Production of METTL3-14 truncated protein complex for crystallography has been based on
344 previously published data[31]. Untagged METTL3 (354-580) and His-tagged METTL14 (107-
345 395) were synthetically cloned into the vector pTriIJ-HV (Evotec). Recombinant virus was
346 produced for each protein and BIICs generated and stored at -80°C. For expression, Sf21 cells
347 grown in Sf900II SFM media plus 5 µg/ml gentamicin were infected with both, METTL3 and
348 METTL14 P2 BIICs at an MOI of 1 (0.5 + 0.5). The infected culture was incubated for 72h at
349 27°C with shaking at 110 rpm, before harvesting by centrifugation and storing at -80°C.
350 Thawed cells were lysed in 20 mM Tris pH 8.0, 200 mM KCl, 10% glycerol, 0.4% Triton-X
351 100 and 5 mM imidazole supplemented with Complete EDTA-free protease inhibitor tablets
352 (Roche) and 10 u/ml Benzonase. Samples were homogenised for 20-30 s with an IKA Ultra-
353 Turrax and sonicated in a Branson probe sonicator (cycles of 30s on, 30s off for 4 minutes at
354 40% amplitude). Sample was centrifuged at 45,000 rpm for 45 min to remove insoluble
355 material and loaded on 5 ml HisTrap FF column, washed with 20 mM Tris pH 8.0, 200 mM
356 KCl, 10% glycerol, 20 mM imidazole and eluted with 0-100% gradient of 20 mM Tris pH 8.0,
357 200 mM KCl, 10% glycerol, 300 mM imidazole over 20 CV. TEV cleavage was carried out
358 with dialysis o/n at 4°C (20 mM Tris pH 8.0, 200 mM KCl, 10% glycerol, 5 mM imidazole),
359 at TEV ratio 1:50; in the presence of 3 mM reduced/oxidised glutathione mixture. This was
360 followed by subtractive affinity chromatography using 1 ml HisTrap FF and size-exclusion on
361 a 16/60 S200 column (20 mM Tris pH 8.0, 200 mM KCl). Purified protein complex was
362 concentrated to 11 mg/ml and snap-frozen in liquid nitrogen for storage at -80°C.
363
364 **X-ray crystallography: Crystallisation and soaking**
365 Protein complex was diluted two-fold with 200 mM KCl and after centrifugation, mixed at 1:1
366 ratio with 200 mM Mg acetate and 20% w/v PEG3350. Crystals grew after several days at RT
367 in both, hanging and sitting drops, and contained SAH carried over from insect cells. Seeding
368 was used to improve crystals reproducibility. To replace SAH with STM2457, crystals were
369 transferred into reservoir solution with 5 mM compound (5% DMSO) for incubation o/n at RT.
370 This was followed by transfer into a fresh drop of soaking solution for another 6 h and
371 subsequent cryo-protection in soaking solution supplemented with 15% glycerol before flash-
372 freezing.
373
374 **X-ray crystallography: Data collection and structure determination**
375 Data was collected to 3 Å at Diamond Light Source I04-1 beamline and processed using
376 Aimless[32]. PDB 5L6D was used as Phaser[33] molecular replacement model. Iterative cycles of
377 refinement using REFMAC5[34] and model building using Coot (v10.11.4)[35] were performed.
378 STM2457 was fitted and restraints created using SMILES string and AFITT[36]. Final structure
379 statistics can be found in Supplementary Table 7, 2% of residues are Ramachandran outliers.
380 The structure was deposited with PDB access code 7O2I.
381
382
383 **STM2457 selectivity profiling**
384 The selectivity profile of STM2457 was assessed by testing the level of inhibition in a panel of
385 methyltransferases and kinases. Inhibition of 4 RNA methyltransferases was tested at Evotec
386 AG, Hamburg using RFMS assays equivalent to the METTL3 assay described above. The IC_{50}
387 was determined from a dilution series of STM2457 with a top concentration of 120 µM and
388 the degree of inhibition at 10µM compound was inferred from this. Additionally, the level of
389 inhibition of a panel of 41 DNA and protein methyltransferases was assessed in a radiometric
390 assay measuring substrate methylation using tritiated SAM by Reaction Biology (Malvern, PA)
391 at 10 µM STM2457 in duplicate. Data were plotted using GraphPad Prism (Version 9).

392 Selectivity testing against 489 kinases was carried out using a binding assay by KINOMEscan,
393 DiscoverX (Eurofins) at 10 µM STM2457 in duplicate.
394
395

396 **METTL3 cellular target engagement**

397 Cellular target engagement of STM2457 was measured by thermal shift using the InCell Pulse
398 Assay (DiscoverX). HeLa cells were transfected with pICP-hMETTL3-eLP (human METTL3
399 Met1-Leu580) or pICP-mMETTL3-eLP (mouse METTL3 Met1-Leu580), using Fugene HD
400 (Promega, #E2311) following the supplier's protocol. 24 hours post transfection, cells were
401 frozen and stored in liquid nitrogen until the day of the assay. On the day of the assay 100 nL
402 compound dilutions (11 point 3-fold dilutions, top concentration in assay: 25 µM) were spotted
403 into the assay plate (Greiner Dilution, 384-well, PP, transparent, #784201). The transfected
404 cells were thawed in a water bath at 37°C and cryoprotectant was exchanged with Opti-MEM
405 lacking phenol red (Gibco, Cat #11058-021). 20 µL of the cell suspension was added to each
406 well of the assay plate to give a final cell number of 1360 cells/well. Plates were sealed with
407 aluminium foil and incubated for 1 hour at 37°C. Afterwards, plates were incubated for 15
408 minutes upside down in a water bath at 45°C, further incubated for 10 minutes at room
409 temperature, and finally centrifuged briefly to gather the liquid in the bottom of each well.
410 Subsequently, 25 µL of detection solution (InCELL Hunter Detection Kit, DiscoverX, #96-
411 0079L; working solution: 16.7 v/v EA reagent, 16.7 v/v lysis buffer and 66.7% substrate
412 reagent) was added to each well and the solution was transferred to the measurement plate
413 (Corning, 384-well, PS, black, Flat Bottom, #3575). The plate was sealed with aluminium foil
414 and incubated at room temperature and slow shaking for 30 minutes. Finally, the assay plate
415 was centrifuged for 1 minute at 100 x g and room temperature and luminescence was measured
416 using an EnVision multimode plate reader (Perkin Elmer). Dose response curves were obtained
417 from three biological replicates. All data in this section were plotted using GraphPad Prism
418 (Version 9).
419

420 **Cell culture**

421 MOLM-13, THP-1, NOMO-1, EOL-1, KASUMI-1 and HL-60 were cultured in RPMI-1640
422 (Invitrogen) supplemented with 10% FBS (Life Technologies) and 1%
423 penicillin/streptomycin/glutamine. OCI-AML2 and OCI-AML3 were cultured in alpha-MEM
424 (Lonza) supplemented with 20% FBS (Life Technologies) and 1%
425 penicillin/streptomycin/glutamine. HPC-7 was cultured in IMDM (Invitrogen) supplemented
426 with 10% FBS, 100ng ml-1 SCF (Peprotech), 7.48 x 10-5 M 1-thioglycerol (Sigma), 1%
427 penicillin/streptomycin/glutamine. 32D was cultured in RPMI (Invitrogen) supplemented with
428 10% FBS, 10 ng ml-1 IL-3 (Peprotech) and 1% penicillin/streptomycin/glutamine. 293T were
429 cultured in DMEM (Invitrogen) supplemented with 10% FBS (Life Technologies) and 1%
430 penicillin/streptomycin/glutamine. HeLa cells were cultured in MEM Eagle culture medium
431 (10% FBS, 2 mM L-Glutamine, 1% NEAA) at 37°C and 5% CO2. All cancer cell lines were
432 obtained from the Sanger Institute Cancer Cell Collection and negative for mycoplasma
433 contamination. Human cell lines employed are not listed in the cross-contaminated or
434 misidentified cell lines database curated by the International Cell Line Authentication
435 Committee (ICLAC).
436

437 **Isolation of haematopoietic progenitors**

438 *Flt3*$^{ITD/+}$ mice[37] were kindly provided by Gary Gilliland and crossed with *Rosa26*$^{Cas9/+}$ mice.
439 Freshly isolated bone marrow from 6- to 10-week-old female *Rosa26*$^{Cas9/+}$, *Flt3*$^{ITD/+}$*;*
440 *Rosa26*$^{Cas9/+}$ or moribund *Npm1*$^{flox-cA/+}$*; Flt3*$^{ITD/+}$, *Npm1*$^{flox-cA/+}$*; Nras*$^{G12D/+}$ mice were used.
441 Bone marrow cells were exposed to erythrocyte lysis (BD PharmLyse, BD Bioscience),

442 followed by magnetic bead selection of Lin⁻ cells using the Lineage Cell Depletion Kit
443 (Miltenyi Biotec) according to the manufacturer's instructions. Lin⁻ were cultured in X-VIVO
444 20 (Lonza) supplemented with 5% FBS (Life Technologies) 10ng ml^{-1} IL3 (Peprotech), 10ng
445 ml^{-1} IL6 (Peprotech) and 50ng ml^{-1} of SCF (Peprotech). Retrovirus constructs pMSCV-MLL-
446 AF9-IRES-YFP and pMSCV-MLL-ENL-IRES-Neo were used with package plasmid psi-Eco
447 to produce retrovirus. 293T cells (Life Technologies) were cultured and prepared for
448 transduction in 10 cm plates. For virus production, 5 µg of the above plasmids and 5 µg psi-
449 Eco packaging vector were transfected drop wise into the 293T cells using 47.5 µl TransIT
450 LT1 (Mirus) and 600 µl Opti-MEM (Invitrogen). The resulting viral supernatant was harvested
451 as previously described. Transduction of primary mouse cells was performed in 6-well plates
452 as mentioned above. After transduction, transduced cells were sorted for YFP (for MLL-AF9)
453 or selected with neomycin (for MLL-ENL).
454 For in vivo experiments related to Extended Data 8, 6 to 10-week-old female $Rosa26^{Cas9/+}$ mice
455 were treated daily for two weeks with either vehicle or 50 mg/kg STM2457 (STORM). Four
456 weeks post-treatment, bone marrow cells from these mice was freshly dissected (as mentioned
457 above) and blocked with anti-mouse CD16/32 (BD Pharmigen, cat. no. 553142) and 10%
458 mouse serum (Sigma). For the identification of LK/LSK and LT-HSC staining was performed
459 using CD4 PE/Cy5 (Biolegend, cat. no. 100514), CD5 PE/Cy5 (Biolegend, cat. no. 100610),
460 CD8a PE/Cy5 (Biolegend, cat. no. 100710), CD11b PE/Cy5 (Biolegend, cat. no. 101210),
461 B220 PE/Cy5 (Biolegend, cat. no. 103210), TER-119 PE/Cy5 (Biolegend, cat. no. 116210),
462 GR-1 PE/Cy5 (Biolegend, cat. no. 108410), SCA-1 Pacific Blue (Biolegend, cat. no. 122520),
463 CD150 PE/Cy7 (Biolegend, cat. no. 115913), CD34 FITC (BD Pharmigen, cat. no. 553733)
464 and CD117 APC-eFluor780 (eBioscience, cat. no. 47-1171). In each of the multi-colour flow
465 cytometry experiments we included the fluorescence minus one (FMO) controls. FMO controls
466 provides a measure of spillover in a given channel. This allows for correct gating and selection
467 of only the stained cells in the experimental sample. Flow cytometry analysis was performed
468 using a LSRFortessa instrument (BD) and resulting data were subsequently analyzed using
469 FlowJo (v10, BD).
470 For blood counts, 20 µl of blood was collected from the tail-vein of the mice using a capillary
471 pipette containing anticoagulants (EDTA). The EDTA anti-coagulated blood samples were
472 used to obtain a complete blood count with a Hemavet Mascot Multispecies Hematology
473 System Counter 1500R (CDC Technologies, Inc., Oxford, CT). Samples were counted no
474 longer than five minutes after blood was drawn.
475 For re-plating assays using the STM2457 inhibitor, 10,000 lineage negative cells and primary
476 murine AML cells were plated in three wells of 6-well-plate of M3434 methylcellulose (Stem
477 Cell Technologies) in the presence of 1µM STM2457. The colonies were counted 7 days later
478 and further 10,000 cells re-seeded and re-counted after a week until the 3rd replating. All data
479 in this section were plotted using GraphPad Prism (version 9).
480
481 **Flow cytometry analyses of AML cells**
482 Cells were treated with vehicle (DMSO) or STM2457 and stained at the indicated timepoints
483 with anti-mouse CD11b PE/Cy5 (Biolegend, cat. no. 101210) and anti-human CD11b PE
484 (eBiosciences, cat. no. 9012-0118). Data were analyzed using LSRFortessa (BD) and FlowJo
485 (v10, BD).
486 Apoptosis levels were measured in human and/or mouse AML cells treated with vehicle
487 (DMSO) or STM2457 at indicated timepoints, using Annexin V (Life Technologies, cat. no.
488 V13242). Data were analyzed by using LSRFortessa (BD) instruments.
489 Cell cycle levels were measured in human and/or mouse AML cells treated with vehicle
490 (DMSO) or STM2457 at indicated timepoints, by using bromodeoxyuridine (BrdU) using the

491 FITC BrdU Flow Kit (BD Pharmingen, 559619) or the APC BrdU Flow Kit (BD Pharmigen,
492 51-9000019AK). Data were analyzed by using LSRFortessa (BD) instruments.
493 For PDX experiments related to Figure 4 and Extended Data 6, 6- to 10-week-old NSG female
494 mice were injected with 10^6 patient-derived AML cells by intravenous injection. For primary
495 transplants, indicated doses of STM2457 or vehicle were delivered to the mice via
496 intraperitoneal injection (IP) on day 5 (PDX-2) or day 10 post-transplant (PDX1,3), once daily
497 for total 12 or 14 days (12-14 treatments). Then bone marrow and spleen cells from these mice
498 were freshly dissected (as mentioned above) and flow-cytometry analysis was performed after
499 staining with Alexa Fluor® 700 CD45 (Biolegend, cat. no. 368513), PE CD93 (eBioscience™,
500 cat. no. 12093841), PerCP/Cyanine5.5 CD33 (Biolegend, cat. no. 303414), APC CD34 Clone
501 8G12 (Biolegend, cat. no. 345804), APC/Cyanine7 CD38 (Biolegend, cat. no. 303533), Biotin
502 anti-human CD19 (Biolegend, cat. no. 302203), Biotin anti-human CD3 (Biolegend, cat. no.
503 300403), Brilliant Violet 605™ CD123 (Biolegend, cat. no. 306025), Brilliant Violet 421™
504 CD45RA (Biolegend, cat. no. 304129), PE/Cy7 CD90 (Biolegend, cat. no. 328123) and
505 streptavidin SA BV510 (Biolegend, cat. no. 405233).
506 For primary and secondary transplantation experiments using primary murine *MLL-*
507 *AF9/Flt3*$^{ITD/+}$, 6- to 10-week-old NSG female mice were injected with 10^6 AML cells by
508 intravenous injection. For primary transplants, indicated doses of STM2457 or vehicle were
509 delivered to the mice via intraperitoneal injection (IP) on day 7 post-transplant, once daily for
510 total 10 days. Then bone marrow cells from these mice was freshly dissected (as mentioned
511 above) and blocked with anti-mouse CD16/32 (BD Pharmigen, cat. no. 101323) and 10%
512 mouse serum (Sigma). For the identification of L-GMP and CD93 populations, staining was
513 performed using Brilliant Violet 711 CD11b (Biolegend, cat. no. 101241), Brilliant Violet 605
514 Gr15 (Biolegend, cat. no. 108439), APC-CD48 (Biolegend, cat. no. 103411), APC-eFluor 780
515 CD117 (eBioscience™ cat. no. 47117182), Biotin Ly-6A/E (Sca-1) (Biolegend, cat. no.
516 108103), Biotin anti-mouse CD127 (IL-7Rα) (Biolegend, cat. no. 135005), Biotin Cd3, B220,
517 Ter119 (Biolegend, cat. no. 559971) and PE CD93 (Biolegend, cat. no. 136503). In each of the
518 multi-colour flow cytometry experiments we included the fluorescence minus one (FMO)
519 controls. FMO controls provide a measure of spillover in a given channel. This allows for
520 correct gating and select only the stained cells in the experimental sample. Flow cytometry
521 analysis was performed using a LSRFortessa instrument (BD) and resulting data were
522 subsequently analyzed using FlowJo (v10, BD). All data in this section were plotted using
523 GraphPad Prism (Version 9).
524
525 **Adult primary leukemia and cord blood sample drug and proliferation assays**
526 All cord blood samples were obtained with informed consent (REC 07-MRE05-44) under the
527 approval of East of England - Cambridge South Research Ethics Committee. Cord-blood-
528 derived CD34+ cells were tested for colony-forming efficiency in StemMACS HSC-CFU
529 semi-solid medium (Miltenyi Biotec) in the presence of the indicated concentration of
530 STM2457 or DMSO. Colonies were counted by microscopy 12–14 days (CD34+ cells) after
531 plating. All data in this section were plotted using GraphPad Prism (Version 9).
532
533 **Western blot analysis**
534 Cells were treated with Vehicle (DMSO) or the indicated concentrations of STM2457 and after
535 72 hours cell pellets resuspended in whole cell lysis buffer (50 mM Tris-HCl pH=8, 450 mM
536 NaCl, 0.1% NP-40, 1mM EDTA), supplemented with 1 mM DTT, protease inhibitors (Sigma),
537 and phosphatase inhibitors (Sigma). Protein concentrations were assessed by Bradford assay
538 (Bio-Rad) and an equal amount of protein was loaded per track. Prior to loading, the samples
539 were supplemented with SDS-PAGE sample buffer and DTT was added to each sample. 10-

540 40 μg of protein was separated on SDS-PAGE gels, and blotted onto polyvinylidene difluoride
541 membranes (Millipore).
542

543 **Drug and Proliferation Assays**

544 All suspension cells were plated in 96-well plates in triplicate at 5,000–10,000 cells per well
545 and treated for 72 hours with vehicle or the indicated concentrations of STM2457 and
546 STM2120 (0.04-50 μM). On day 4, an equal volume for all wells was split using fresh media
547 and compound, such that the resulting cell density in each well matched the initial seeding
548 density. Plates were measured on day 6 using CellTiter 96 AQueous Non-Radioactive Cell
549 Proliferation Assay (Promega) in order to calculate the relative cell proliferation. All the
550 compounds were dissolved in DMSO.
551 For the rescue experiments, cDNA was obtained by reverse transcription of MOLM13 cell
552 RNA with Supercript III (ThermoFisher Scientific), then the SP1 full-length coding sequence
553 was amplified by PCR and cloned into pHIV-ZsGreen plasmid (Addgene 18121) by Gibson
554 assembly (Gibson Assembly Cloning Kit, NEB), using the HpaI site. MOLM13 cells were
555 transduced with the SP1 or empty lentiviral vectors, then GFP+ cells were isolated by flow
556 cytometry sorting after 4 days and employed in proliferation and western blot assays as
557 descripted above. All data in this section were plotted using GraphPad Prism (Version 9).
558

559 **Antibodies**

560 Western blot experiments were performed using the following antibodies: anti-METTL3 from
561 Bethyl Laboratories (A301-568A), anti-METTL14 from Abcam (ab98166), anti-DICER1 from
562 Abcam (ab14601), anti-DDX3X from Abcam (ab128206), anti-ACTIN from Abcam (ab8227),
563 anti-BRD4 (N-term) from Abcam (ab128874), anti-BRD4 (C-term) from Bethyl Laboratories
564 (A301-985A), anti-BCL2 from Abcam (ab32124), anti-SP1 from Merck (07-645), anti-
565 HNRNPL from Abcam (ab6106), anti-c-MYC from Santa Cruz Biotechnology (sc5605) and
566 anti-GAPDH from Santa Cruz Biotechnology (sc47724) and Goat anti-Rabbit from Cell
567 Signaling Technology (7074S). HRP activity was revealed using the SuperSignal™ West Pico
568 Plus kit (ThermoScientific, 34580). For the m^6A-RIP experiments the following antibodies
569 were used: anti-N6-methyladenosine antibody (m^6A), clone 17-3-4-1 from Merck (MABE
570 1006) and IgG Isotype Control from Merck (NI03).
571

572 **Generation and bioluminescent imaging of primary murine and PDX models**

573 Generation of AML PDX models and lentiviral transduction for transgenic expression of
574 enhanced firefly luciferase was performed as described in detail by Vick, et al. [38]. For primary
575 and secondary transplantation experiments using primary murine *MLL-AF9/Flt3$^{ITD/+}$*, 6- to 10-
576 week-old NSG female mice were injected with 10^6 AML cells by intravenous injection.
577 Indicated doses of STM2457 or vehicle were delivered to the mice via intraperitoneal injection
578 (IP) on day 10 post-transplant, once daily for total two weeks (14 treatments). STM2457 was
579 dissolved in 20%(w/v) 2-hydroxyproply beta-cyclodextrin vehicle (Sigma, H107). At day 10
580 post-transplant, the tumor burdens of the animals were detected using IVIS Lumina II (Caliper)
581 with Living Image version 4.3.1 software (PerkinElmer). Briefly, 100 μl of 30 mg/ml D-
582 luciferin (BioVision) was injected into the animals intraperitoneally. Ten min after injection,
583 the animals were maintained in general anesthesia by isoflurane and put into the IVIS chamber
584 for imaging. The detected tumor burdens were measured and quantified by the same software.
585 Diseased mice were assessed blindly by qualified animal technicians from the Sanger mouse
586 facility. Mice were housed in specific pathogen-free conditions in the Wellcome Sanger
587 Institute animal facilities. All cages were on a 12:12-h light:dark cycle (lights on, 07:30) in a
588 temperature-controlled and humidity-controlled room. Room temperature was maintained at
589 72 ± 2 °F (22.2 ± 1.1 °C), and room humidity was maintained at 30–70%. The animals were

590 culled when the tumor burden was 10^9 photons per second or higher. All animal studies were
591 carried out in accordance with the Animals (Scientific Procedures) Act 1986, UK and approved
592 by the Ethics Committee at the Sanger Institute. Randomization and blinding were not applied.
593 All data in this section were plotted using GraphPad Prism (Version 9).
594
595 **STM2457 pharmacokinetic analysis**
596 Three C57BL6/J mice were given IP injections of 30 mg/kg STM2457 and sampled serially up
597 to 24 hours after dosing. Blood was collected from the tail vein at the indicated timepoints.
598 Plasma was isolated by centrifugation, and 20 µL of plasma or blood was mixed with a
599 precipitant solution of 120 µL acetonitrile and internal standard. Supernatant from this
600 precipitation was diluted 1:1 v/v in water and 2.5 uL injections were characterised by LC-MS
601 on a TSQ triple quadrupole mass spectrometer attached to an Accela pump (Thermo) and an
602 HTS-CTC PAL autosampler. STM2457 was resolved on Hypersil Gold C18 solid phase (30 X
603 2.1 mm, 1.9 µm particles, Thermo) with an increasing gradient of 5-95% B over 30 seconds.
604 Mobile phases consisted of 0.1% formic acid in water (A) and acetonitrile (B) and the flow
605 was held at 1.0 ml/min. Blood to plasma ratio was determined using results from the
606 appropriate samples, and the LLOQ was set at 10 ng/ml. All data in this section were plotted
607 using GraphPad Prism (Version 9).
608
609 **RNA nucleoside quantification by mass spectrometry**
610 For Figures 1g-h and Extended Data 2c, MOLM-13 cells were grown in RPMI-1640
611 supplemented with 10% fetal bovine serum and maintained in culture between 0.3 and 1.5 x
612 10^6 cells/ml. Cells were treated with Vehicle (DMSO) or 1 µM STM2457 for the timepoints
613 indicated (24 hours for 1G and 1H, 48 hours for S1C). For animal experiments related to
614 Extended Data 6 and 7, 6- to 10-week-old NSG female mice were injected with 1 x 10^6 patient-
615 derived AML cells by intravenous injection. Indicated doses of STM2457 or vehicle were
616 delivered to the mice via IP on day 5 (PDX-2) or 8 post-transplantation (PDX1,3), once daily
617 for total 12 or 14 days, respectively. Then, whole bone marrow from these mice was dissected
618 and AML cells were purified using flow sorting (hCD45 or YFP). For *in vivo* experiments
619 related to Extended Data 8, 6 to 10-week-old female Rosa26$^{Cas9/+}$ mice were treated daily for
620 two weeks with either vehicle or 50 mg/kg STM2457 (STORM) and whole bone marrow from
621 these mice was dissected. Subsequent total RNA extraction from cells of all origins was
622 performed using the RNeasy Mini Kit (Qiagen) and polyA+ RNA was purified using a
623 Dynabeads mRNA purification kit (Invitrogen), in both cases following the manufacturer's
624 recommendations. Nucleosides were prepared from all poly A+ RNA by addition of nuclease
625 digest mix. Each 100 uL volume contained 62.5 units of Benzonase (Sigma Aldrich), 5 units
626 of Antarctic Phosphatase (NEB) and 10 mU/µL of Phosphodiesterase I (PDEI) from *Crotalus*
627 *adamanteus* venom (Sigma Aldrich) made up in a buffer composed of 20 mM Tris-HCl (pH
628 8), 20 mM MgCl2 and 100 mM NaCl. Nucleosides were liberated by digestion at 37ºC
629 overnight. The following morning the sample was cooled to room temperature and 100 µl of
630 ice cold 2x Mass Spec buffer was added (0.1% formic acid containing internal standard).
631 In all cases, nucleosides were quantified by LC-MS using a Sciex 4500 triple quadrupole mass
632 spectrometer attached to either a U3000 or 1290 liquid chromatograph (Thermo Scientific or
633 Agilent, respectively). Nucleosides were separated across a HSS T3 column (2mm x 10mm
634 with 1.8 µm particles, Waters) using an increasing gradient of 2-15% mobile phase B. The
635 mobile phases were 0.1% v/v formic acid in water or acetonitrile for mobile phase A and B,
636 respectively, and the flow was held at 300 µL/min. Nucleoside concentrations were
637 extrapolated from a concentration curve of external standards and expressed as modified
638 nucleoside relative to the total amount of canonical nucleosides. All data in this section were
639 plotted using GraphPad Prism (Version 9).

640
641 **Polysome fractionation**
642 5×10^7 MOLM-13 cells treated with vehicle (DMSO) or 1µM STM2457 for 72 hours and then
643 further treated with 0.1 mg ml^{-1} cycloheximide for 5 min at 37°C. Then they were lysed and
644 polysomes were fractionated on a sucrose gradient as previously described[39]. Relative RNA
645 abundance in each fraction was then quantified by RT–qPCR. All data in this section were
646 plotted using GraphPad Prism (Version 9).
647
648 **Quantitative RT–PCR**
649 Total RNA or RNA isolated from the polysome fractions or the m^6A immunoprecipitation
650 assays was isolated from MOLM-13 cells using the RNeasy Mini Kit (Qiagen). For cDNA
651 synthesis, total RNA was reverse-transcribed with the SuperScript VILO cDNA Synthesis kit
652 (Life Technologies). The levels of specific RNAs was measured using the Step One Plus real-
653 time PCR machine (Applied Biosciences) and the Fast SYBRGreen PCR mastermix (Applied
654 Biosciences) according to the manufacturer's instructions. For experiments related to Figure
655 3f-g and Extended Data 5f, the *BRD4*, *SP1*, *DICER1 and METTL3* mRNA levels were
656 normalized to, the housekeeping gene, *GAPDH*. For experiments related to Extended Data 5f,
657 the *BRD4*, *SP1, BCL2, HOXA10, ARPC5* and *DDX3X* mRNA levels were normalized were
658 normalized to IgG control groups. All samples, including the template controls, were assayed
659 in triplicates. The relative quantification of target gene expression was performed with the
660 standard curve or comparative cycle threshold (C_T) method. The primer sequences are listed in
661 the Supplementary Table 6. All data in this section were plotted using GraphPad Prism
662 (Version 9).
663
664 **m^6A RNA immunoprecipitation and sequencing**
665 Total RNA was isolated from MOLM-13 cells treated with vehicle (DMSO) or 1 µM STM2457
666 or 48 hours using the RNAeasy midi kit (Qiagen). Successively polyA+ RNA was purified
667 from 300 µg total RNA using Dynabeads mRNA purification kit (Invitrogen). 500 ng of
668 polyA+ purified RNA was used for each immunoprecipitation reaction. m^6A RNA
669 immunoprecipitation was performed using the Magna MeRIP m^6A kit (Millipore) according
670 to the manufacturer's instructions.
671 Single-end 50-bp stranded libraries and sequenced using HiSeq 2500. Multiplexed reads were
672 split on the basis of their barcodes using Illumina Basespace. Reads were trimmed to remove
673 the TruSeq adaptor using trim_galore with parameters '-q 0 -a
674 AGATCGGAAGAGCACACGTCTGAACTCCAGTCAC–phred33–fastqc'.
675 Read quality was assessed using FastQC (v11.8)[40] To control for ribosomal contamination,
676 reads were first mapped to hg38 rDNA sequences using bwa (v7.17) (default parameters) and
677 reads that matched were removed from downstream analyses. The remaining read data were
678 filtered for PCR duplicates using SAMtools (v1.10)[41].
679 Filtered non-ribosomal reads were next mapped to the hg38 genome using hisat2 (v2.1) with
680 default parameters[42]. Mapped reads were filtered to remove those mapping to more than one
681 unique genomic locus (multihits) by keeping only reads with flag NH:i:1 in the output bam file
682 from hisat2 (v2.1). Reads were further filtered to remove the ones with mapping quality less
683 than 20 using SAMtools (v1.10). Genome coverage bedgraph files were generated using
684 genomeCoverageBed from the BEDTools (v2.27.1) suite of tools[43]. Coverage files were
685 converted to bigwig format using bedGraphToBigWig (v377). Statistical analysis and results
686 of differentially methylated peaks in vehicle- and STM2457-treated cells was performed using
687 the R package MeTDiff (v1.0)[44] and the GENCODE human gene annotation GRCh38 v97
688 from Ensembl and are provided in Supplemental Table 3. Metagene plots were generated using
689 the R/Bioconductor package Guitar (v2.2.0)[45]. Peak and RNA overlaps illustrated in Extended

Data Fig. 5A, B are presented in Supplemental Table 4 and the relevant data from MOLM13 with METTL3 knockdown were derived from previously published study[6]. The m^6A peaks were analysed for enrichment of known and *de novo* motifs using the software HOMER (v4.10)[46]. Genes that showed significant differential m^6A were further tested for Gene Ontology (GO) enrichment of known Biological Processes (BP) using the R/Bioconductor package clusterProfiler (v3.14.3)[47]. Functional enrichment results are provided in Supplemental Table 5.

RNA sequencing

Input samples from the m^6A RNA immunoprecipitation experiments were used to characterize the transcriptional profiles of vehicle versus STM2457-treated cells. The RNA-seq analysis of the input samples (vehicle n=2, STM2457 n=2) was performed using the nf-core/rnaseq bioinformatics pipeline (workflow container 1.4.2) under default parameters with hisat2 as the specified aligner[48]. Differential gene expression analysis was conducted using the R/Bioconductor package DESeq2 (v1.26.0)[49]. Genes showing an absolute log-fold change greater than one (|log2FoldChange | > 0.5) at an adjusted p-value for False Discovery Rate (FDR) less than 0.05 (padj < 0.05) were defined as being differentially expressed between vehicle and STM2457-treated cells. Results of the differential expression analyses between these two conditions (padj ≤ 0.05) are given in Supplemental Table 1. Functional profiling of the differentially expressed genes was performed using over-representation and Gene Set Enrichment Analyses (GSEA) of GO terms (Domain: Biological Process) and annotated gene sets available in the Molecular Signatures Database (MSigDB), as implemented in the R/Bioconductor package clusterProfiler (v3.14.3)[47]. Functional enrichment results for the down-regulated genes (log2FoldChange ≤ 0.7, padj < 0.05) are given in Supplemental Table 2.

Statistical analysis

Statistical analyses performed using two-tailed Student's T-test, log-rank (Mantel–Cox) test (for survival comparisons) and one-way Anova, all included in the figure legends. Results were considered significant for a p-value (or adjusted p-value when multiple testing) below 0.05. Statistical significance of the overlap between two groups of gene sets were computed using Fisher's exact test using the R/Bioconductor package GeneOverlap (v1.22)[50].

Data accessibility

The datasets related to STM2457 used in this study can be accessed from ENA: PRJEB41662. The previously published datasets from Barbieri *et al* can be accessed from the Gene Expression Omnibus database with accession number GSE94613.
The STM2457 structure is deposited with PDB access code 7O2I. Additional details related to the chemical characterisation of STM2457 could be found in the relevant published patent (WO2020201773) on WIPO.

REFERENCES

31 Sledz, P. & Jinek, M. Structural insights into the molecular mechanism of the m(6)A writer complex. Elife 5, doi:10.7554/eLife.18434 (2016).

32 Evans, P. R. & Murshudov, G. N. How good are my data and what is the resolution? Acta Crystallogr D Biol Crystallogr 69, 1204-1214, doi:10.1107/S0907444913000061 (2013).

740 33 McCoy, A. J. et al. Phaser crystallographic software. J Appl Crystallogr 40, 658-674,
741 doi:10.1107/S0021889807021206 (2007).
742 34 Winn, M. D., Murshudov, G. N. & Papiz, M. Z. Macromolecular TLS refinement in
743 REFMAC at moderate resolutions. Methods Enzymol 374, 300-321,
744 doi:10.1016/S0076-6879(03)74014-2 (2003).
745 35 Emsley, P. & Cowtan, K. Coot: model-building tools for molecular graphics. Acta
746 Crystallogr D Biol Crystallogr 60, 2126-2132, doi:10.1107/S0907444904019158
747 (2004).
748 36 Wlodek, S., Skillman, A. G. & Nicholls, A. Automated ligand placement and
749 refinement with a combined force field and shape potential. Acta Crystallogr D Biol
750 Crystallogr 62, 741-749, doi:10.1107/S0907444906016076 (2006).
751 37 Lee, B. H. et al. FLT3 mutations confer enhanced proliferation and survival properties
752 to multipotent progenitors in a murine model of chronic myelomonocytic leukemia.
753 Cancer Cell 12, 367-380, doi:10.1016/j.ccr.2007.08.031 (2007).
754 38 Vick, B. et al. An advanced preclinical mouse model for acute myeloid leukemia
755 using patients' cells of various genetic subgroups and in vivo bioluminescence
756 imaging. PLoS One 10, e0120925, doi:10.1371/journal.pone.0120925 (2015).
757 39 Panda, A. C., Martindale, J. L. & Gorospe, M. Polysome Fractionation to Analyze
758 mRNA Distribution Profiles. Bio Protoc 7, doi:10.21769/BioProtoc.2126 (2017).
759 40 Andrews, S. (Available online
760 http://www.bioinformatics.babraham.ac.uk/projects/fastqc, 2010).
761 41 Li, H. et al. The Sequence Alignment/Map format and SAMtools. Bioinformatics 25,
762 2078-2079, doi:10.1093/bioinformatics/btp352 (2009).
763 42 Kim, D., Paggi, J. M., Park, C., Bennett, C. & Salzberg, S. L. Graph-based genome
764 alignment and genotyping with HISAT2 and HISAT-genotype. Nat Biotechnol 37,
765 907-915, doi:10.1038/s41587-019-0201-4 (2019).
766 43 Quinlan, A. R. & Hall, I. M. BEDTools: a flexible suite of utilities for comparing
767 genomic features. Bioinformatics 26, 841-842, doi:10.1093/bioinformatics/btq033
768 (2010).
769 44 Cui, X. et al. MeTDiff: A Novel Differential RNA Methylation Analysis for MeRIP-
770 Seq Data. IEEE/ACM Trans Comput Biol Bioinform 15, 526-534,
771 doi:10.1109/TCBB.2015.2403355 (2018).
772 45 Cui, X. et al. Guitar: An R/Bioconductor Package for Gene Annotation Guided
773 Transcriptomic Analysis of RNA-Related Genomic Features. Biomed Res Int 2016,
774 8367534, doi:10.1155/2016/8367534 (2016).
775 46 Heinz, S. et al. Simple combinations of lineage-determining transcription factors
776 prime cis-regulatory elements required for macrophage and B cell identities. Mol Cell
777 38, 576-589, doi:10.1016/j.molcel.2010.05.004 (2010).
778 47 Yu, G., Wang, L. G., Han, Y. & He, Q. Y. clusterProfiler: an R package for
779 comparing biological themes among gene clusters. OMICS 16, 284-287,
780 doi:10.1089/omi.2011.0118 (2012).
781 48 Ewels, P. A. et al. The nf-core framework for community-curated bioinformatics
782 pipelines. Nat Biotechnol 38, 276-278, doi:10.1038/s41587-020-0439-x (2020).
783 49 Love, M. I., Huber, W. & Anders, S. Moderated estimation of fold change and
784 dispersion for RNA-seq data with DESeq2. Genome Biol 15, 550,
785 doi:10.1186/s13059-014-0550-8 (2014).
786 50 Shen, L. & ISoMaM', S. (Available online, http://shenlab-sinai.github.io/shenlab-
787 sinai/, 2020).
788
789

Acknowledgments

T.K. was supported by grants from Cancer Research UK (grant reference RG17001) and ERC (project number 268569), in addition to benefiting from core support from the Wellcome Trust (Core Grant reference 092096), Cancer Research UK (grant reference C6946/A14492) and Kay Kendall Leukaemia Fund project grant (grant reference RG88664). K.T. was funded by a Wellcome Trust Sir Henry Wellcome Fellowship (grant reference RG94424). K.T and M.E. were funded by Leukaemia UK (G108148). I.J. was funded by ERC (Consolidator Grant 681524). I.J. and K.T. were funded by Cambridge-LMU Strategic Partnership Award. G.S.V. was funded by a Cancer Research UK Senior Cancer Fellowship (C22324/A23015). We thank Bee Ling Ng, Jennifer Graham, Sam Thompson and Christopher Hall for help with flow cytometry and the Cambridge Blood and Stem Cell Biobank for human AML and cord blood sample processing; the staff of the Sanger Institute Core Sequencing facility for sequencing and the staff of the Sanger Institute Research Support Facility for help with mouse experiments. We thank David Hardick, Beth Thomas, Yaara Ofir-Rosenfeld and Alexandra Sapetschnig at Storm Therapeutics for comments and advice, and Kerstin Danker, Mark Ridgill, Coralie Hoareau, and their colleagues at Evotec for drug discovery services and lead optimization support.

Author Contributions

K.T., T.K. and O.R. conceived the study and designed the experiments; K.T., W.B., E.Y., M.A., E.S.P., D.A., J.R., E.D.B, M.G., D.L., A.G.H., B.A., R.S., N.A.W., R.F., P.G. and M.E. conducted chemical, biochemical and molecular experiments. K.T., E.Y., J.R., E.D.B and M.G. performed animal experiments. G.T. and J.M.L.D. performed bioinformatics analyses. E.S.P. performed x-ray crystallography, assisted by W.B. in data analysis and interpretation. E.Y. and D.A. performed polysome profiling with help and supervision from N.I. and K.T. A.J.B., I.J. and G.S.V. helped with data analysis, interpretation and direction. K.T., T.K., E.Y., M.E. and O.R. wrote the manuscript with help from all authors. All authors discussed the results and commented on the manuscript.

Competing interests

T.K. is a co-founder of Abcam Plc and Storm Therapeutics Ltd, Cambridge, UK and Scientific Advisor to Foghorn Therapeutics and EpiVario. E.Y. is funded by Storm Therapeutics Ltd, Cambridge, UK. W.B., M.A., G.T., D.L., B.A., R.F., A.G.H., N.A.W., P.G. and O.R. are employees of Storm Therapeutics Ltd, Cambridge, UK. E.S.P. is an employee of Evotec (UK) Ltd, Abingdon, UK. George S. Vassiliou is a consultant for Kymab, Cambridge, UK. Storm Therapeutics Ltd is the owner of a patent application (WO2020201773) covering the development of METTL3 RNA methyltrasferase inhibitors.

Correspondence and requests for materials

Ane correspondence or requests for materials related to this study should be addressed to K.T., T.K. or O.R..

Fig.1: Characterisation of the RNA methyltransferase inhibitor STM2457.

a) Chemical structure of STM2457. b) Biochemical activity assay showing inhibition of the METTL3/14 enzyme complex using a dose-range of STM2457 and STM2120. c) Surface plasmon resonance (SPR) assay showing binding affinity of STM2457 to the METTL3/14 protein complex. d) SPR assay showing binding affinity to the METTL3/METTL14 protein

840 complex is reduced in the presence of SAM, indicative of SAM-competitive binding. e)
841 STM2457 inhibits METTL3/METTL14 selectively in a methyltransferase profiling panel of
842 45 RNA (red bars), DNA (green bars) and protein methyltransferases (grey bars) (red star
843 indicates <50% activity remaining) (n=2). f) Crystal structure of METTL3/METTL14
844 (carbon atoms in green) in complex with STM2457 (carbon atoms in cyan). Hydrogen bonds
845 (yellow dashed lines) and water molecules proximal to the inhibitor (red sphere) are shown
846 (PDB code 7O2I). g) Quantification of m^6A levels on poly-A^+-enriched RNA after 24 hours
847 of treatment of MOLM-13 with the indicated STM2457 concentrations (mean +/- s.d., n=3).
848 IC_{50}, half maximum inhibitory concentration.
849
850
851 **Fig.2: Pharmacological inhibition of METTL3 affects AML cells.**
852 a) Dose-response curves of an AML cell line panel to STM2457 (mean +/- s.d., n=3). b) Colony
853 forming efficiency of primary murine *MLL-AF9/Flt3*$^{Itd/+}$ and NPM1c/*Flt3*$^{Itd/+}$ AML cells
854 treated with vehicle or STM2457 (mean +/- s.d., n=3). Half maximum inhibitory concentration
855 (IC_{50}) per cell line is illustrated in brackets. c) Colony forming efficiency of WT Lin^- cells
856 treated with vehicle or STM2457 (mean +/- s.d., n=3). d) CD11b and Mac1 levels of MOLM-
857 13 and *MLL-AF9/Flt3*$^{Itd/+}$ primary murine cells, respectively, treated with vehicle or STM2457.
858 e) BrdU staining and cell cycle analysis in MOLM-13, HPC7 and *MLL-AF9/Flt3*$^{Itd/+}$ primary
859 murine cells treated with vehicle or STM2457. f) Percentage of apoptotic cells in a human
860 AML cell line panel, following treatment with STM2457 at the indicated time-points (mean
861 +/- s.d., n=3). g) Western blot analysis of BRD4, c-MYC, SP1 and GAPDH in MOLM-13 cells
862 treated with the indicated doses of STM2457 or vehicle (n=3). two-tailed Student's t-test; $*P$
863 < 0.01; $**P < 0.0001$, n.s. not significant; WT, wild-type.
864
865
866 **Fig.3: STM2457 reduces m^6A levels and causes mRNA translation defects.**
867 a) Genomic distribution of all m^6A peaks called (left) and/or the genomic distribution of
868 downregulated m^6A peaks (right) on poly-A^+-enriched RNAs from STM2457-treated MOLM-
869 13 cells. b) The distribution of all (red) or down-regulated (light blue) m^6A peaks of MOLM-
870 13 cells upon treatment with STM2457. c) Motif analysis of the sequences under depleted
871 peaks, following treatment with STM2457 (hypergeometric test). d) Genomic visualization of
872 the m^6A-meRIP normalized signal for *SP1*, *MYC* and *HOXA10* in MOLM13 cells following
873 treatment with vehicle or STM2457. e) Polysome fractionation analysis in MOLM-13 cells
874 treated with vehicle or STM2457. Absorbance was continuously measured at 254 nm. f) RT-
875 qPCR quantification of *SP1*, *BRD4* and *DICER1* mRNAs in each polysome fraction presented
876 as a percentage of total mRNA (mean +/- s.d., n=3). g) RT-qPCR quantification of *SP1* and
877 *BRD4* in total RNA samples isolated from MOLM-13 cells treated with vehicle or STM2457
878 (mean +/- s.d., n=3). UTR, untranslated region; CPG, CPG island; TSS, transcription start site;
879 CDS, coding sequence; nm, nanometres; MW, molecular weight; n.s., not significant; two-
880 tailed Student's t-test; $*P < 0.05$.
881
882
883 **Fig.4: STM2457 prevents AML expansion and reduces key leukaemia stem cells *in vivo*.**
884 a) Bioluminescence imaging of AML PDX-1 (*NPM1c*) treated with vehicle or 50 mg/kg
885 STM2457 (n=5). b) Kaplan-Meier survival of AML PDX-1 (*NPM1c*) after treatment with
886 vehicle or 50 mg/kg STM2457 at indicated times (n=5). c) Bioluminescence imaging of AML
887 PDX-2 (*MLL-AF6*) treated with vehicle or 50 mg/kg STM2457 (n=5). d) Kaplan-Meier
888 survival of AML PDX-2 (*MLL-AF6*) after treatment with vehicle or 50 mg/kg STM2457 at
889 indicated times (n=5). e) Percentage of $CD45^+$ cells in live bone marrow and spleen after

890 treatment with vehicle or 50 mg/kg STM2457 (n=5). f) Percentage of $CD93^+$ on $CD38^-/CD34^+$
891 cells in bone marrow after treatment with vehicle or 50 mg/kg STM2457 (n=5). g) Kaplan-
892 Meier survival after re-transplantation of AML PDX-2 (MLL-*AF6*) which was treated with
893 vehicle or 50 mg/kg STM2457 at indicated times (n=5). Treatment (in red) and non-dashed
894 lines in red or black refer to the primary transplantation illustrated in Fig. 4d. h) Percentage of
895 human $CD45^+$ cells in peripheral blood after re-transplantation of AML PDX-2 (MLL-*AF6*)
896 (n=5). Related to Fig. 4g. PBC, peripheral blood count; d, day; two-tailed Student's t-test; Log-
897 rank (Mantel–Cox) test was used for survival comparisons.
898
899
900 **Extended Data Figure. 1**
901 **STM2457 is a specific small molecule inhibitor of METTL3 with no evidence of off-**
902 **target effects.**
903 a) Chemical structures of STM1760 and STM2120. b) Biochemical activity assay showing
904 inhibition of the METTL3/METTL14 enzyme complex using a dose-range of STM1760. c)
905 Surface plasmon resonance (SPR) sensorgram showing the binding of STM2457 to the
906 METTL3/METTL14 protein complex. d) SPR sensorgram showing reduced binding of
907 STM2457 to the METTL3/METTL14 protein complex in the presence of 50 μM SAM,
908 illustrating that STM2457 is SAM competitive. e) SPR assay showing single-cycle binding
909 kinetics of STM2457. f) Biochemical activity assay showing no inhibition of METTL16,
910 NSUN1 and NSUN2 RNA methyltransferases using a dose-range of STM2457. g)
911 Methyltransferase dendrograms showing that 10 μM STM2457 has selective inhibitory activity
912 for METTL3/METTL14 over the indicated RNA and protein methyltransferases. h) Treatment
913 with 10 μM STM2457 did not inhibit (ie result in less than 50% control activity) any of the
914 468 kinases in the ScanMax (DiscoverX) kinase panel tested (marked by green dots).
915
916
917 **Extended Data Figure. 2**
918 **Binding of STM2457 to the SAM pocket of METTL3.**
919 a) Overlay of crystal structures of METTL3/METTL14 in complex with STM2457 (carbon
920 atoms in cyan) and METTL3/14 in complex with SAM (carbon atoms in magenta, PDB code
921 7O2I). The position of K513 is shown in lines of the corresponding color for each structure.
922 b) Cellular thermal shift target engagement assay measuring binding affinity of STM2457
923 against human and mouse METTL3 proteins expressed in HeLa cells. The IC_{50} represents the
924 concentration of STM2457 at which 50% of METTL3 is bound to STM2457. (mean +/- s.d.,
925 n=3). c) Quantification of m^6A levels on poly-A^+-enriched RNA using RNA-mass
926 spectrometry after 48 hours of *in vitro* treatment of MOLM-13 with 1 μM of STM2457 or
927 vehicle (DMSO). (mean +/- s.d., n=3). d) Quantification of m^6A_m, m^6_2A and m^7G levels on
928 poly-A^+-enriched RNA 24 hours of treatment of MOLM-13 with the indicated STM2457
929 concentrations (mean +/- s.d., n=3). e) STM2457 *in vivo* pharmacokinetic profile in mouse
930 blood and brain tissue using a dose of 50 mg/kg. f) STM2457 *in vivo* PK/PD relationship in
931 non-tumour bearing animals from the PK study shown in (e), demonstrating inhibition of m^6A
932 in spleen tissue over a range of STM2457 blood concentrations (n=3). two-tailed Student's t-
933 test.
934
935
936 **Extended Data Figure. 3 Treatment with STM2457 triggers colony forming deficiency**
937 **and apoptosis in AML cells.**
938 a) Colony-forming efficiency of CD34+ human cord blood cells ($n = 3$) in the presence of 1, 5,
939 or 10 μM STM2457 (mean $\pm$ s.d., n=3). These changes are not significant at the 95%

940 confidence level according to one-way Anova on repeated measures. Error bars refer to
941 variation across 3 different individuals (blue, brown and red square). b) Proliferation assay in
942 MOLM-13 cells after treatment with the indicated doses of STM2457 and STM2120,
943 illustrating no sensitivity to the latter at any tested dose (mean ± s.d., n=3). c) Colony forming
944 efficiency of primary murine *MLL-ENL/Flt3*$^{ITD/+}$ and NPM1c/*NRAS-G12D* AML cells treated
945 with 1 μM STM2457 showing decreased clonogenic potential compared with vehicle-treated
946 (DMSO) controls (mean ± s.d., n=3). d) Mac1 levels were used to assess differentiation of non-
947 leukaemic haemopoietic cell line HPC7. Flow cytometry comparison on day 4 post-treatment
948 between vehicle (DMSO) and 1 μM STM2457. e) Selective increased apoptosis in AML cells
949 but not in non-leukaemic haematopoietic cells, following treatment with 1 μM of STM2457 at
950 the presented time points (mean ± s.d., n=3). f) Western blot for SP1 and ACTIN in MOLM-
951 13 cells transduced with plasmids expressing *SP1* cDNA or an empty control (n=3). g) Dose-
952 response curves of MOLM-13 cells to STM2457 after transduction with vectors expressing
953 *SP1* cDNA or an empty control, showing selective decrease of drug sensitivity upon ectopic
954 expression the former. The dose-response curve of parental MOLM-13 (WT, light blue) shown
955 in Fig. 2a is illustrated for comparison purposes. (mean ± s.d., n = 3). d, days; two-tailed
956 Student's t-test; *$P < 0.05$, **$P < 0.01$
957
958
959 **Extended Data Figure. 4 Differential expression analysis of AML cells after treatment**
960 **with STM2457.**
961 a) Volcano plot for MOLM13 cells treated with 1 μM STM2457 versus control samples after
962 48 hours of treatment, showing significantly dysregulated genes in red (Padj ≤ 0.01). b)
963 Extended gene ontology analysis of the differentially expressed genes post-treatment with 1
964 μM STM2457 in MOLM-13 cells. c) Representative GO signatures of the differentially
965 expressed genes post-treatment with STM2457 in MOLM-13 cells. LFC, Log Fold Change.
966
967
968 **Extended Data Figure. 5**
969 **Pharmacological inhibition of METTL3 significantly reduces m^{6}A on leukaemia-**
970 **associated substrates**
971 a) Overlap between METTL3-dependent m^{6}A poly-A$^+$ RNAs in MOLM-13 cells either treated
972 with 1 μM STM2457 or with genetic downregulation of METTL3 from Barbieri *et al*[7]. b)
973 Overlap between differential downregulated m^{6}A peaks in MOLM-13 cells either treated with
974 1 μM STM2457 or with genetic downregulation of METTL3 from Barbieri et al[7]. c) Genomic
975 visualization of the m^{6}A-meRIP normalized signal in MOLM13 cells following treatment with
976 vehicle (DMSO) or 1 μM STM2457 for the METTL3-dependent m^{6}A substrates *BRD4* and
977 *HNRNPL* (red stars indicate loss of m^{6}A signal). d) m^{6}A-meRIP-qPCR analysis of METTL3-
978 dependent and METTL3-independent m^{6}A substrates normalized to input in MOLM-13 cells
979 treated for 24 or 48 hours with either vehicle (DMSO) or 1 μM STM2457 (mean ± s.d., n=3).
980 e) Gene ontology analysis of differentially m^{6}A-methylated mRNAs upon treatment with 1 μM
981 STM2457. f) RT-qPCR quantification of *METTL3* and *DICER1* in total RNA samples from
982 MOLM-13 cells treated with vehicle or STM2457 (mean +/- s.d., n=3). g) Western blot for
983 METTL3, METTL14, DDX3X, DICER1 and ACTIN in MOLM-13 cells treated with 10, 5
984 and 1 μM of STM2457 or vehicle (DMSO) for 72 hours (n=3). two-tailed Student's t-test; n.s.,
985 not significant; KD, knockdown.
986
987
988
989 **Extended Data Figure. 6**

990 **STM2457 shows high efficacy and strong target engagement in PDX models.**
991 a) Quantification of luminescence for the animal experiment depicted in Fig. 4a (mean ± s.d,
992 n=5). b) Bioluminescence imaging of mice transplanted with AML PDX-3 (*MLL-AF10)*
993 treated with vehicle or 50 mg/kg STM2457 (n=5). c) Kaplan-Meier survival of AML PDX-3
994 (*MLL-AF10*) following 12 consecutive treatments with vehicle or 50 mg/kg STM2457 at
995 indicated times (n=5). d) Quantification of luminescence for the animal experiment depicted
996 in Extended Data Fig. 4c (mean ± s.d, n=5). e) Quantification of luminescence for the animal
997 experiment depicted in Fig. 4c (mean ± s.d, n=5). f) Body weight for the animal experiment
998 depicted in Fig. 4a (n=5). Statistical significance was determined by two-tailed Mann–Whitney
999 U test and box plots showing median, IQR and extremes. g) Western blot for SP1, BRD4,
1000 HNRNPL, BCL2, METTL3 and ACTIN protein levels in AML PDX-3 (*MLL-AF6*) treated
1001 with vehicle or 50 mg/kg STM2457 (n=4). h) RNA-mass spectrometry quantification of m^6A
1002 levels on poly-A^+-enriched RNA from bone marrow of AML PDX-3 (*MLL-AF10*) treated *in*
1003 *vivo* with vehicle, 30 mg/kg STM2457 or 50 mg/kg STM2457 (mean ± s.d., n=4). D, day; n.s.
1004 not significant; two-tailed Student's t-test; Log-rank (Mantel–Cox) test was used for survival
1005 comparisons.
1006
1007
1008 **Extended Data Figure. 7**
1009 **STM2457 treatment is efficacious and targeted in primary murine AML.**
1010 a) Percentage of YFP^+ *MLL-AF9/Flt3*$^{Itd/+}$ cells in the bone marrow of mice treated with vehicle
1011 or 30 mg/kg STM2457 (mean ± s.d., n=4). b) Spleen weight of *MLL-AF9/Flt3*$^{Itd/+}$ murine AML
1012 models following treatment with vehicle or 30 mg/kg STM2457 (mean ± s.d., n=4). c) Western
1013 blot showing SP1, BRD4, HNRNPL, BCL2, METTL3 and ACTIN protein levels in murine
1014 AML (*MLL-AF9/Flt3*$^{Itd/+}$) models treated with either vehicle or 30 mg/kg STM2457 (n=4). d)
1015 RNA-mass spectrometry quantification of m^6A levels on poly-A^+-enriched RNA *in vivo* from
1016 AML murine models (*MLL-AF9/Flt3*$^{Itd/+}$) treated with vehicle, 30 mg/kg STM2457 or 50
1017 mg/kg STM2457 (mean ± s.d., n=4). e) Percentage of $CD93^+$ cells in the bone marrow of *MLL-*
1018 *AF9/Flt3*$^{Itd/+}$ murine models following treatment with either vehicle or 30 mg/kg STM2457
1019 (mean ± s.d., n=5). f) Percentage of L-GMP cells in the bone marrow of *MLL-AF9/Flt3*$^{Itd/+}$
1020 murine models following treatment with either vehicle or 30 mg/kg STM2457 (mean ± s.d.,
1021 n=5). g) CD48 levels of L-GMP cells in the bone marrow of *MLL-AF9/Flt3*$^{Itd/+}$ murine models
1022 following treatment with either vehicle or 30 mg/kg STM2457 (mean ± s.d., n=5). h) Kaplan-
1023 Meier survival after re-transplantation of cells isolated from primary transplanted animals with
1024 *MLL-AF9/Flt3*$^{Itd/+}$ treated and treated with either vehicle or 30 mg/kg STM2457 (n=5). i)
1025 Percentage of YFP^+ cells in the peripheral blood 12 days after re-transplantation with *MLL-*
1026 *AF9/Flt3*$^{Itd/+}$ (mean ± s.d., n=5). D, day; BM, bone marrow; PBC, peripheral blood count; n.s.
1027 not significant; two-tailed Student's t-test; Log-rank (Mantel–Cox) test was used for survival
1028 comparisons.
1029
1030
1031 **Extended Data Figure. 8**
1032 **Pharmacological inhibition of METTL3 has no lasting effects on normal haematopoiesis.**
1033 a-c) Quantification of LSK (Lin-/$Ska1^+$/c-Kit^+) and HSC (LSK/$CD150^+$/$CD34^-$) compartments
1034 in bone marrow from WT C57BL/6J mice following 14 consecutive daily treatments with
1035 either vehicle or 50 mg/kg STM2457 (mean ± s.d., n=5). d) Blood count results from animal
1036 experiments related to a-c. e) Body weight of mice from animal experiments related to a-d (n
1037 = 5). Statistical significance was determined by two-tailed Mann–Whitney U test and box plots
1038 showing median, IQR and extremes. f) RNA-mass spectrometry quantification of m^6A levels
1039 on poly-A^+-enriched RNA from healthy bone marrow related to the animal experiments a-d,

1040 following 14 days of consecutive treatments with either vehicle or 50 mg/kg STM2457 (mean
1041 ± s.d., n=5). HSC, hematopoietic stem cells; two-tailed Student's t-test; n.s., not significant.

a

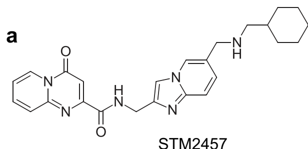

b

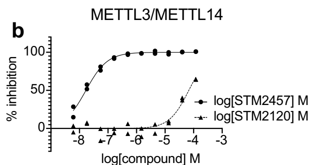

c

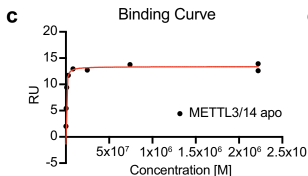

d

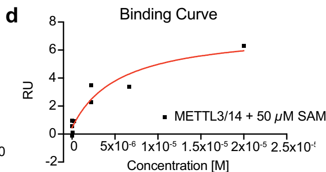

e

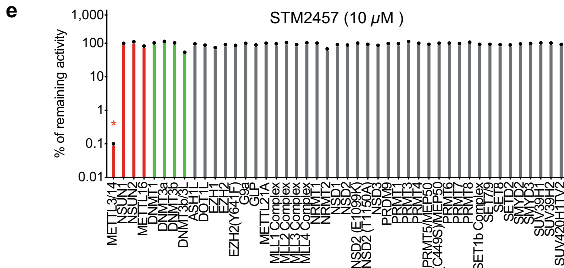

f

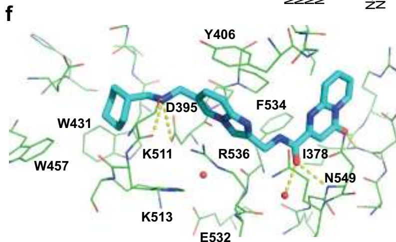

g

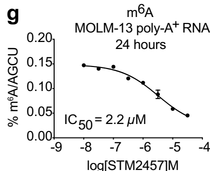

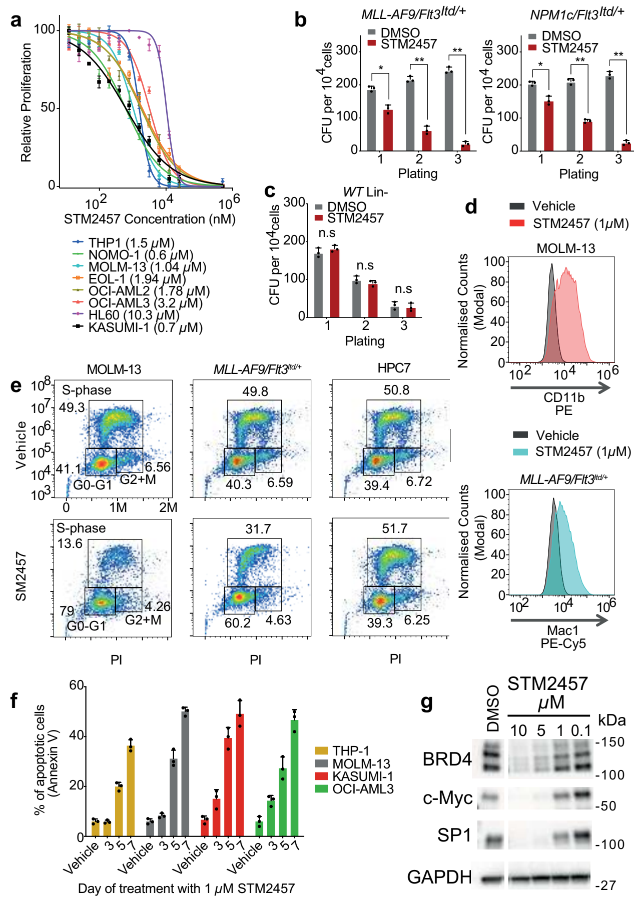
a
Relative Proliferation
STM2457 Concentration (nM)
THP1 (1.5 μM)
NOMO-1 (0.6 μM)
MOLM-13 (1.04 μM)
EOL-1 (1.94 μM)
OCI-AML2 (1.78 μM)
OCI-AML3 (3.2 μM)
HL60 (10.3 μM)
KASUMI-1 (0.7 μM)
b
MLL-AF9/Flt3ltd/+
NPM1c/Flt3ltd/+
DMSO
STM2457
CFU per 10^4 cells
Plating
c
WT Lin-
n.s
d
Vehicle
STM2457 (1μM)
MOLM-13
Normalised Counts (Modal)
CD11b PE
Mac1 PE-Cy5
e
HPC7
S-phase
G0-G1
G2+M
Vehicle
SM2457
PI
f
% of apoptotic cells (Annexin V)
THP-1
MOLM-13
KASUMI-1
OCI-AML3
Day of treatment with 1 μM STM2457
g
DMSO
STM2457 μM
kDa
BRD4
c-Myc
SP1
GAPDH

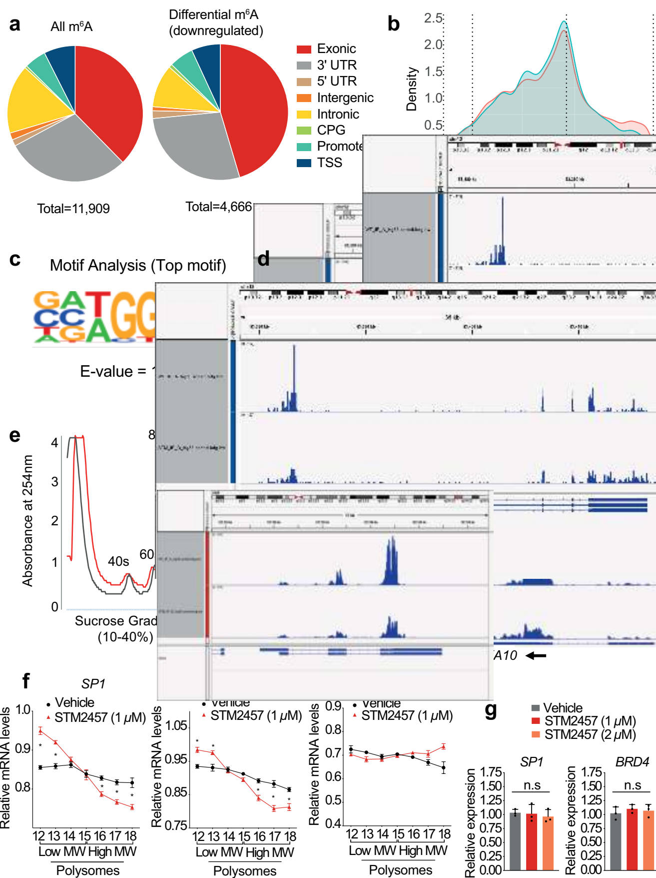

a
All m6A
Differential m6A (downregulated)
Exonic
3' UTR
5' UTR
Intergenic
Intronic
CPG
TSS
Total=11,909
Total=4,666
b
Density
c
Motif Analysis (Top motif)
d
e
Absorbance at 254nm
40s
60
Sucrose Grad
(10-40%)
f
SP1
Vehicle
STM2457 (1 μM)
Relative mRNA levels
Low MW High MW
Polysomes
g
Vehicle
STM2457 (1 μM)
STM2457 (2 μM)
SP1
BRD4
n.s
Relative expression

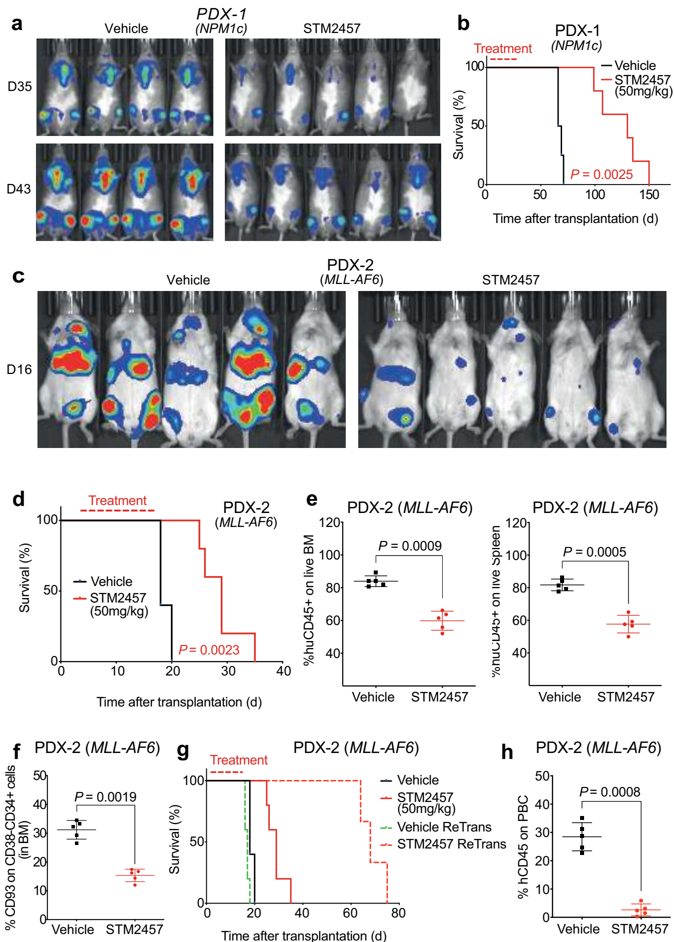

a
PDX-1
(NPM1c)
Vehicle
STM2457
D35
D43
b
PDX-1
(NPM1c)
Treatment
Vehicle
STM2457
(50mg/kg)
Survival (%)
P = 0.0025
Time after transplantation (d)
c
PDX-2
(MLL-AF6)
Vehicle
STM2457
D16
d
Treatment
PDX-2
(MLL-AF6)
Survival (%)
Vehicle
STM2457
(50mg/kg)
P= 0.0023
Time after transplantation (d)
e
PDX-2 (MLL-AF6)
%huCD45+ on live BM
P = 0.0009
Vehicle
STM2457
PDX-2 (MLL-AF6)
%huCD45+ on live Spleen
P = 0.0005
Vehicle
STM2457
f
PDX-2 (MLL-AF6)
% CD93 on CD38-CD34+ cells (in BM)
P = 0.0019
Vehicle
STM2457
g
PDX-2 (MLL-AF6)
Treatment
Survival (%)
Vehicle
STM2457
(50mg/kg)
Vehicle ReTrans
STM2457 ReTrans
Time after transplantation (d)
h
PDX-2 (MLL-AF6)
% hCD45 on PBC
P= 0.0008
Vehicle
STM2457